Science and Technology of Advanced Materials: Methods

ISSN: 2766-0400 (Online) Journal homepage: www.tandfonline.com/journals/tstm20

Gigacycle fatigue properties of additively manufactured Hastelloy X

Yoshiyuki Furuya, Hideaki Nishikawa, Kota Sawada, Tomotaka Hatakeyama, Masahiro Kusano & Makoto Watanabe

To cite this article: Yoshiyuki Furuya, Hideaki Nishikawa, Kota Sawada, Tomotaka Hatakeyama, Masahiro Kusano & Makoto Watanabe (2026) Gigacycle fatigue properties of additively manufactured Hastelloy X, Science and Technology of Advanced Materials: Methods, 6:1, 2607165, DOI: 10.1080/27660400.2025.2607165

To link to this article: https://doi.org/10.1080/27660400.2025.2607165

Published online: 29 Jan 2026.

SCIENCE AND TECHNOLOGY OF ADVANCED MATERIALS: METHODS
2026, VOL. 6, NO. 1, 2607165
https://doi.org/10.1080/27660400.2025.2607165

Gigacycle fatigue properties of additively manufactured Hastelloy X

Yoshiyuki Furuya, Hideaki Nishikawa, Kota Sawada, Tomotaka Hatakeyama, Masahiro Kusano and Makoto Watanabe

Research Center for Structural Materials, National Institute for Materials Science, Tsukuba, Japan

ABSTRACT

Gigacycle fatigue tests were conducted on additively manufactured (AM) Hastelloy X. Individual AM samples manufactured in the Z and X directions were tested at room temperature, and the results were compared with those for conventionally produced material. The samples were subjected to ultrasonic fatigue testing up to 10^9 cycles and to servo-hydraulic fatigue testing up to 10^7 cycles. The microstructures of the AM samples consisted of (101) texture that showed high internal plastic strain. The 0.2% proof stress levels of the AM samples were much higher than those of the conventional samples. Internal fractures were seen in both the AM and the conventional samples above 10^7 cycles, indicating conventional fatigue limits at 10^7 cycles to be absent in Hastelloy X. The gigacycle fatigue strengths were comparable between the AM and conventional samples and between the Z and X directions. The conventional fatigue test results for the AM samples revealed longer fatigue lives than those for the conventional samples because of the high 0.2% proof stress. These results show the ultrasonic fatigue test results of the AM samples to be continuously connected to the conventional fatigue test results, unlike the gap seen with conventional samples. Conventional fatigue limits at 10^7 cycles appear to be absent in Hastelloy X, with new fatigue limits possible in the gigacycle region. The internal fracture origins in the AM samples were solidification cracks or the matrix itself, meaning that fatigue failure was not caused by porosities or lack of fusion in these AM samples.

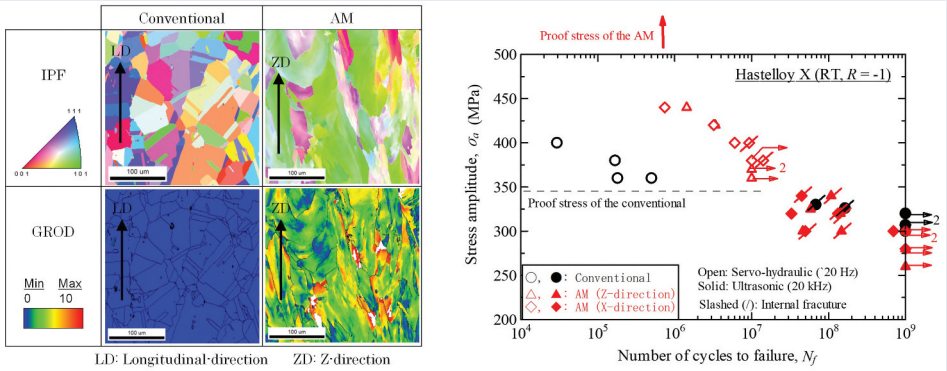

Gigacycle fatigue test results on AM Hastelloy X

ARTICLE HISTORY
Received 20 October 2025
Revised 7 December 2025
Accepted 16 December 2025

KEYWORDS
Gigacycle fatigue; additive manufacturing; Hastelloy X; internal fracture; room temperature

IMPACT STATEMENT

This paper discloses gigacycle fatigue test results on additively manufactured (AM) Hastelloy X. The Hastelloy X revealed internal fractures above 10^7 cycles, indicating conventional fatigue limits at 10^7 cycles to be absent.

1. Introduction

Additively manufactured (AM) metals are valuable materials, since their high degree of design freedom enables the manufacture of components with complex shapes. However, it is crucial to know the fatigue properties for AM metallic materials before applying them in practical contexts. This has made them a focus of major research interest [1–11]. Past investigations have clarified many features of the fatigue properties that are caused by their unique microstructures and defects. One of the characteristics of many types of AM metallic materials is their absence of fatigue limits [12–17]. This has created a need for investigations into these materials of very high cycle fatigue (VHCF) at

CONTACT Yoshiyuki Furuya FURUYA.Yoshiyuki@nims.go.jp Research Center for Structural Materials, National Institute for Materials Science, 1-2-1 Sengen, Tsukuba , Ibaraki 305-0047, Japan

over 10^7 cycles and gigacycle fatigue up to and over 10^9 cycles. This urgent need prompted ASTM to develop recommended practices for VHCF testing [18].

The authors have over 20 years' experience of research into the gigacycle fatigue of metallic materials [19,20]. The key technology has been ultrasonic fatigue testing at 20 kHz [21–27], a technique that enables 10^9 cycles to be applied in a single day, unlike the 3 - 4 months needed for conventional 100-Hz fatigue testing. Frequency effects were initially a concern; however, it has been confirmed that frequency effects are very small in many gigacycle fatigue tests of high-strength metallic materials. In short, ultrasonic fatigue test results show good agreement with conventional fatigue test results for many types of high-strength metallic materials [19,20,25,28–30]. Ultrasonic fatigue testing can also be conducted at high temperatures [31]. Gigacycle fatigue failures are frequently caused by internal fractures, which are fatigue fractures that originate in internal defects. These internal fractures were closely studied, resulting in our proposed new model for predicting gigacycle fatigue strength in which the effects of internal defect sizes can be taken into account [32–34]. This new model can thus be applied to research into gigacycle fatigue in AM metallic materials.

We adopted these techniques in launching research into gigacycle fatigue of AM metallic materials. Our target materials were nickel-based superalloys used for gas turbines. The first material selected was Hastelloy X, a solid-solution hardened type with simple single-phase microstructures. Laser powder bed fusion (LPBF) was the AM technology used. The authors have experience of producing AM Hastelloy X using this technology [35]. The fatigue properties of AM Hastelloy X have been reported for high-cycle fatigue [36–38], for low-cycle fatigue [39] and for crack propagation [40]; however, there was no literature on gigacycle fatigue or VHCF. In this study we conducted gigacycle fatigue tests using ultrasonic fatigue testing and, for comparison, high-cycle fatigue (HCF) tests using a servo-hydraulic fatigue testing machine. These were conducted at room temperature as the first step, so high-temperature gigacycle fatigue tests will be the obvious next step. This report aims for prompt disclosure of these fatigue test data, discussing the validity of the fatigue testing methods. Another point to be discussed in this report is the presence or absence of fatigue limits in AM Hastelloy X, as well as the actual mechanism of fatigue failure.

2. Experimental method

2.1. Materials

AM samples were fabricated using Hastelloy-X powder (AMPERPRINT 0228.074 by Höganäs AB) using an SLM 280 HL (SLM solutions GmbH) commercial SLM machine. Table 1 shows the chemical composition of Hastelloy-X powder. Table 2 shows the LPBF process conditions. Two types of samples, made in the Z- and X-direction, were fabricated as shown in Figure 1. Their geometry consisted of round bars of diameter 15 mm and length 70 mm. These samples were fabricated on a stainless steel baseplate with support structures and were tested without heat treatment, i.e. in their as-built condition.

Conventional Hastelloy X was also tested for comparison. The conventional Hastelloy X consisted of forged round bars of the type described in NIMS creep data sheets [41], designated as heat iHB in creep data sheet No. 55 [42]. Their chemical compositions are also displayed in Table 1.

The microstructures were characterized by electron backscatter diffraction (EBSD), using inverse pole figure (IPF) and grain reference orientation deviation (GROD) maps. The tensile tests were performed at room temperature, to identify 0.2% proof stress, tensile strength, elongation and reduction of area. Young's modulus and density were also evaluated, which were prerequisites to conducting ultrasonic fatigue testing.

Table 1. Chemical compositions of the Hastelloy X samples.

	Element (mass %)											
Sample	C	Si	Mn	*P*	S	Cr	Mo	W	Co	B	Fe	Ni
AM powder	0.05	<0.1	<0.0	<0.002	0.002	21.8	8.9	0.5	1.6	<0.002	18.6	bal.
Conventional	0.06	0.34	0.45	0.01	<0.01	21.4	9.0	0.8	1.2	0.004	17.9	bal.

Table 2. LPBF process conditions.

Process parameters	Value
Laser power, *P*	300 W
Scanning velocity, *v*	909 mm/s
Hatching space, *h*	100 μm
Power layer thickness, *d*	30 μm
Rotation angle of scanning direction	67°
Scan strategy	chessboard scan
Square size in chessboard scan	5×5 mm^2

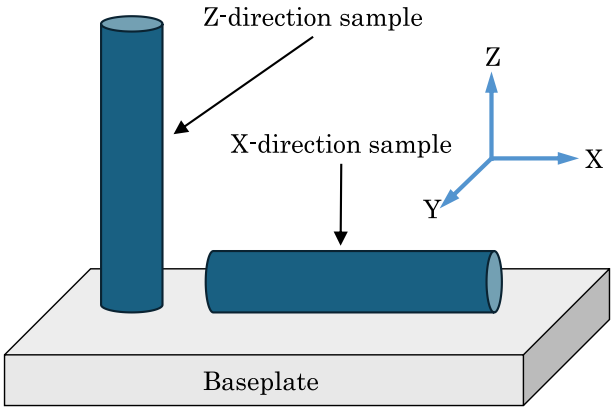

Figure 1. Fabrication of Z- and X-direction samples.

2.2. Fatigue testing

Ultrasonic fatigue testing at 20 kHz was carried out using a commercial-available machine (Shimadzu USF2000). The maximal cycle number tested was 10^9 cycles. The ultrasonic fatigue testing machine was equipped with an air cooling system to minimize temperature increase in the specimens that consisted of a vortex tube-type cooler and a 5.5 kW-class compressor. Intermittent testing [23] was also applied, since too much heat was generated by the Hastelloy X specimens to be limited by air cooling alone. Intermittent test conditions, i.e. pulse/pause ratios, were adopted so as to maintain the specimen's surface temperature, measured using an infrared thermometer and Black-body tape, at below 30°C. The HCF tests, using a servo-hydraulic fatigue testing machine, were conducted under load-controlled conditions. The maximal cycle number tested was 10^7 cycles. The frequencies, ranging from 1–20 Hz, were determined in the same manner as during the intermittent ultrasonic fatigue testing. Both the ultrasonic fatigue and HCF tests were conducted at room temperature in air with a stress ratio of $R = -1$.

Figure 2 shows the dimensions of the fatigue test specimens. The difference between the AM and conventional Hastelloy X specimens was their length, designed to have them resonate at 20 kHz. The specimen length was determined by measuring the resonance frequencies of three different lengths of the specimens. These specimens were subjected to both the ultrasonic fatigue tests and to the HCF tests, i.e. the same geometries of the specimens were used in the ultrasonic fatigue and HCF tests. The specimens were machined from above-mentioned round bars of the AM and conventional Hastelloy X samples, meaning that the surface roughness characteristic of the AM processes was removed. The narrowed areas of the specimen surfaces were finished by longitudinal polishing with 1200-grade silicon carbide paper. The fracture surfaces of the specimens were observed using a scanning electron microscope (SEM), and the microstructures beneath the fracture surfaces were evaluated by cross-sectional EBSD analysis.

3. Experimental results

3.1. Microstructure and tensile properties

Figure 3 shows the microstructures evaluated by EBSD. The IPF maps are for the longitudinal direction (LD) and Z-direction (ZD) in the conventional and AM Hastelloy X samples, respectively. The IPF maps indicated that the AM samples had a (101) texture, in contrast to the random texture of the conventional samples. The GROD maps are drawn using the same contour range. It was concluded from the GROD maps that internal plastic strain was much greater in the AM samples than in the conventional samples. Identifiable defects such as cracks and pores were not found in these microstructure observations. The AM microstructure observations at much higher magnification revealed cellular structures within the grains as described in Section 3.3. Although the AM microstructures shown in Figure 3 are for the Z-direction sample, those for the X-direction sample are similar, i.e. the only difference is the loading directions.

Table 3 shows the tensile test results. The tensile properties of the AM Z-direction sample were close to those of the conventional sample except for the 0.2% proof stress. The strong internal strain of the AM samples could result in higher 0.2% proof stress. The AM X-direction sample was revealed to have higher

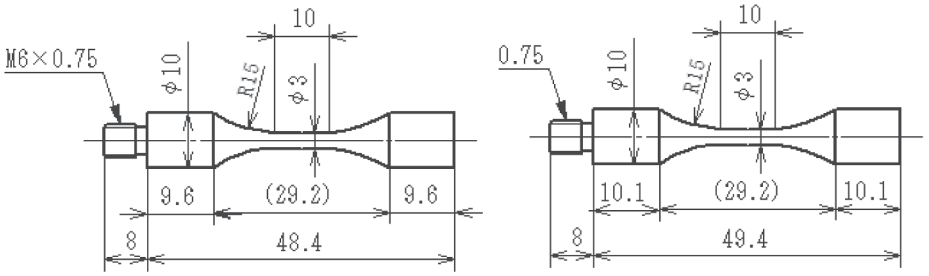

(a) AM Hastelloy X (Z- and X-directions) (b) Conventional Hastelloy X

Figure 2. Profiles of specimens in mm.

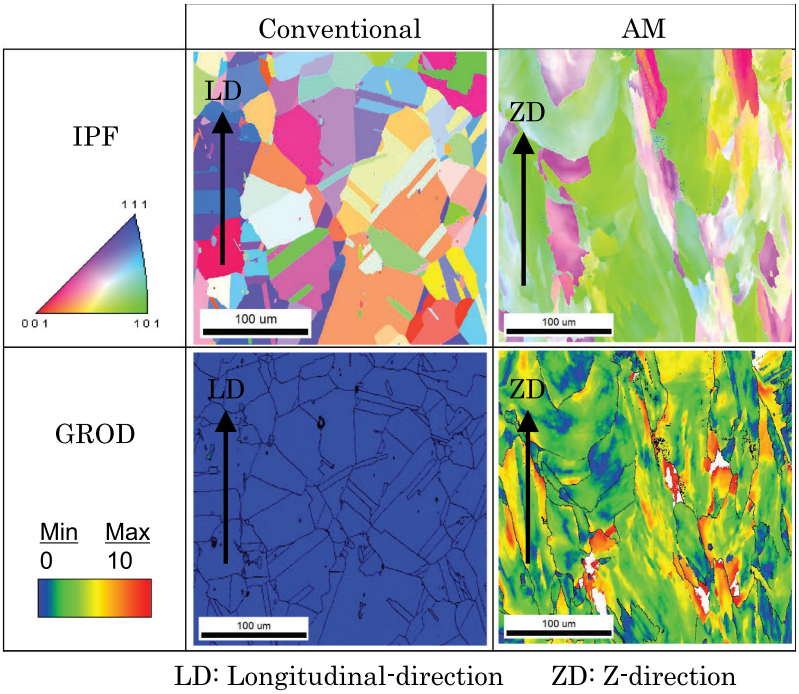

Figure 3. IPF and GROD maps of the tested Hastelloy X.

Table 3. Tensile test results at room temperature.

Sample	Direction	0.2% Proof Stress, MPa	Tensile strength, MPa	Elongation, %	Reduction of Area, %
Conventional	–	344	763	47	66
AM	Z-direction	594	708	43	70
	X-direction	669	863	29	51

strength and lower ductility than the AM Z-direction sample. This anisotropy might be attributable to the (101) texture of the AM samples.

Table 4 shows Young's modulus and density. The Young's modulus was observed, based on the specimen lengths, at the resonance frequency of 20 kHz, as shown in Figure 2. The specimen length resonated at 20 kHz is a function of the Young's modulus and the density. The Young's modulus can, therefore, be reversely calculated from the specimen length when the density is provided [31]. Table 5 shows measured resonance frequencies to determine the specimen lengths. By linearly fitting these data, we calculated the specimen lengths resonated at 20.00 kHz which was the resonance frequency of the used ultrasonic fatigue testing machines without a specimen. The density was estimated by measuring the weight of disks cut out from a 10 mm-diameter section of the specimens. The difference in Young's modulus and density between the AM and the conventional samples was negligible. No anisotropy was observed in the Young's modulus of the AM samples, since the specimen lengths were the same in the Z- and X- directions. The AM samples had a (101) texture, with the Young's modulus of this texture being very close to that of the random texture [43,44].

Table 4. Young's modulus and density.

Sample	Direction	Young's modulus, GPa	Density, g/cm^3
Conventional	–	182	8.13
AM	Z-direction	177	8.22
	X-direction	177	

Table 5. Measured resonance frequencies of three different length of specimens.

Sample	Direction	Specimen length: Total without an external thread, mm	Specimen length: Shoulder part, mm	Resonance frequency, kHz
Conventional	–	49.2	10.0	20.02
		51.2	11.0	19.87
		53.2	12.0	19.76
AM	Z-direction	47.4	9.1	20.06
		49.4	10.1	19.94
		51.4	11.1	19.82
	X-direction	47.4	9.1	20.08
		49.4	10.1	19.92
		51.4	11.1	19.83

3.2. Fatigue properties

Figure 4 shows the fatigue test results. The open and solid marks respectively indicate the HCF and the ultrasonic fatigue test results. The slash marks indicate specimens that ended in internal fractures. The ultrasonic fatigue tests were conducted at below 340 MPa since the temperature of the specimens exceeded 30°C at over 350 MPa even for minimum pulse periods. The HCF tests were conducted at above 360 MPa, since the AM samples reach 10^7 cycles at that stress level. As a result, the ultrasonic fatigue test results did not overlap with the HCF test results.

Most of the specimens subjected to the ultrasonic fatigue tests ended in internal fractures at above 10^7 cycles. Internal fractures also occurred in the HCF tests at around 10^7 cycles, whereas conventional surface fractures could be seen in most of the HCF specimens. Fatigue strengths from the ultrasonic fatigue test results were comparable between the AM and the conventional samples, while in the HCF test results, the AM samples revealed longer fatigue lives than did the conventional samples. The longer fatigue lives of the AM samples subjected to the HCF tests are attributed to their higher 0.2% proof stress. In short, the HCF tests on the conventional samples were conducted at above their 0.2% proof stress, while the 0.2% proof stresses of the AM samples were much higher than under the test conditions. When the stress amplitude exceeds the 0.2% proof stress, macroscopic and cyclic plastic deformation occurs, resulting in decrease of the fatigue lives. As a result, the results for the conventional samples revealed a gap between the HCF and the ultrasonic fatigue test results, unlike the continuous connection seen in the results for the AM samples.

The difference in results between the Z- and X-direction AM samples was minor, both for the HCF tests and for the ultrasonic fatigue tests. The tensile strength of the X-direction AM samples was higher than that of the Z-direction AM samples. Namely, the effects of tensile strength were not observed in the fatigue test results. The difference was also minor between the AM and conventional samples in the ultrasonic fatigue test results despite difference of tensile strength. The effects of tensile strength were thus obscure in these fatigue test results particularly in the VHCF regions. Fatigue strength is normally correlated with tensile strength, so these obscure tensile strength effects could be a characteristic of the AM Hastelloy X. However, the detailed mechanism was not clarified in this study.

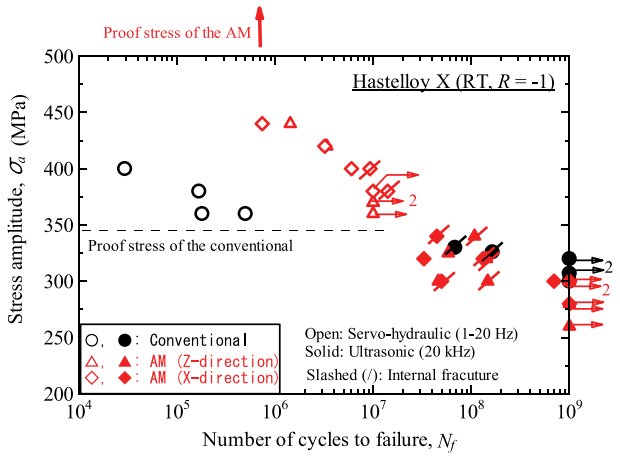

Figure 4. Fatigue test results at room temperature.

3.3. Fracture surfaces

Figure 5 shows typical fracture surfaces at the internal fracture origins. The conventional samples revealed no defects at the internal fracture origins. Flat areas, resembling so-called 'facets' [45,46], were observed at the internal fracture origins. The internal fracture origins of the AM samples were revealed to constitute two types: Type A and Type B. In Type A, a distinctive pattern was observed at the internal fracture origins, whereas Type B did not show this pattern.

Figure 6 shows the results of the cross-sectional EBSD analysis. Three cases: conventional, AM Z-direction (Type A) and AM Z-direction (Type B), were selected for this analysis. The IPF map of the conventional sample indicated that the facet was formed in an inclined direction, close to 45° relative to the loading direction, i.e. very close to the shear direction. The plane on which the facet was formed could match a {111} slip plane. This result suggests the facet to be a shear-type fatigue crack. The GROD map revealed only a slight increase in the internal plastic strain, meaning that the plastic strain induced during the fatigue test was not very high. The IPF map of the AM Z-direction sample (Type A) indicated that the area of the distinctive pattern had been formed in a more inclined direction than the facet of the conventional sample. The direction in which the distinctive pattern area was formed was closer to the Z-direction than to the shear direction. The distinctive pattern area did not match any slip plane. The GROD map was almost identical to that of the initial microstructure shown in Figure 3. The IPF map of the AM Z-direction sample (Type B) indicated that the fracture surface was very flat and that the crack was of a transgranular type. The GROD map did not differ from the initial version.

Figure 7 shows the results of detailed observations of the distinctive patterns. The specimens were the same as those in Figure 5, whereas the fracture surface in the AM Z-direction was on the opposite side and was observed with the specimen tilted. The distinctive patterns of the Z- and X-directions were very similar to each other. Striped patterns were observed in the distinctive pattern area, with small protrusions distributed throughout. Figure 8 shows the microstructure beneath the distinctive pattern area at a much higher

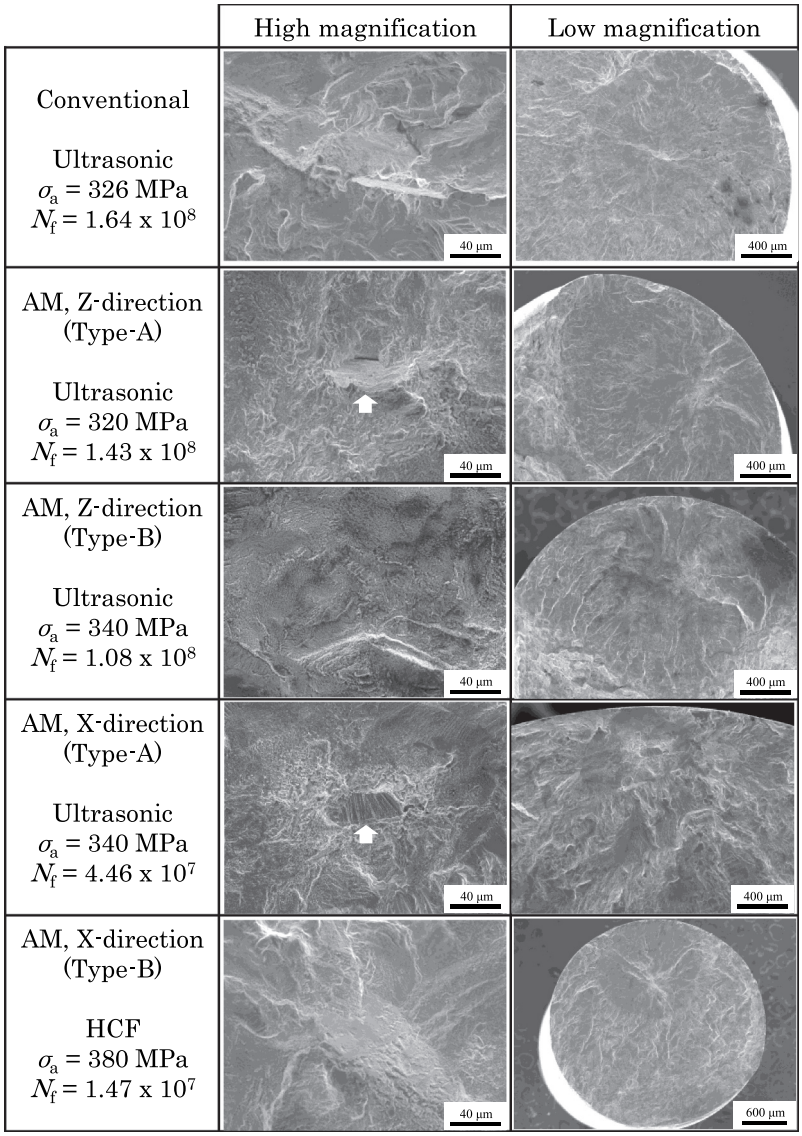

σ_a: Stress amplitude, N_f: Number of cycles to failure

Figure 5. Typical fracture surfaces at internal fracture origins.

magnification, which is a backscattered electron (BSE) image of SEM. At this magnification, cellular structures were observed as reported in the literature [9,47]. These cellular structures were observed everywhere in the microstructure, and the sizes of the cells were close to the width of each stripe that constituted the striped patterns on the fracture surfaces. Figure 9 shows the result of matching the cross-sectional EBSD to the distinctive pattern. This result indicates that the distinctive pattern area was formed at a grain boundary.

4. Discussion

4.1. Fatigue limit and validity of the ultrasonic fatigue testing

The fatigue test results shown in Figure 4 clearly indicate that conventional fatigue limits at 10^7 cycles were absent in the AM Hastelloy X. Many specimens revealed internal fractures at above 10^7 cycles, indicating that the elimination of conventional fatigue limits was attributable to the occurrence of the internal fractures. Its gigacycle fatigue behavior is very similar to that seen in high-strength metallic materials. This was also the case with the conventional Hastelloy X. In short, this gigacycle fatigue behavior is not a distinctive characteristic of the AM version, but an intrinsic characteristic of Hastelloy X.

Our past research on high-strength metallic materials suggests that new fatigue limits were present in the gigacycle regions despite the absence of conventional fatigue limits. New fatigue limits have been confirmed in high-strength steels by conducting gigacycle fatigue tests up to 10^{11} cycles [48]. The presence of new fatigue limits has been suggested in high-strength wrought aluminum alloys [29] and in Ti-6Al-4V alloys [30]. They may also be present in Hastelloy X. Although the fatigue tests were terminated at 10^9 cycles, fatigue failures near 10^9 cycles were very rare, despite many fatigue failures at around

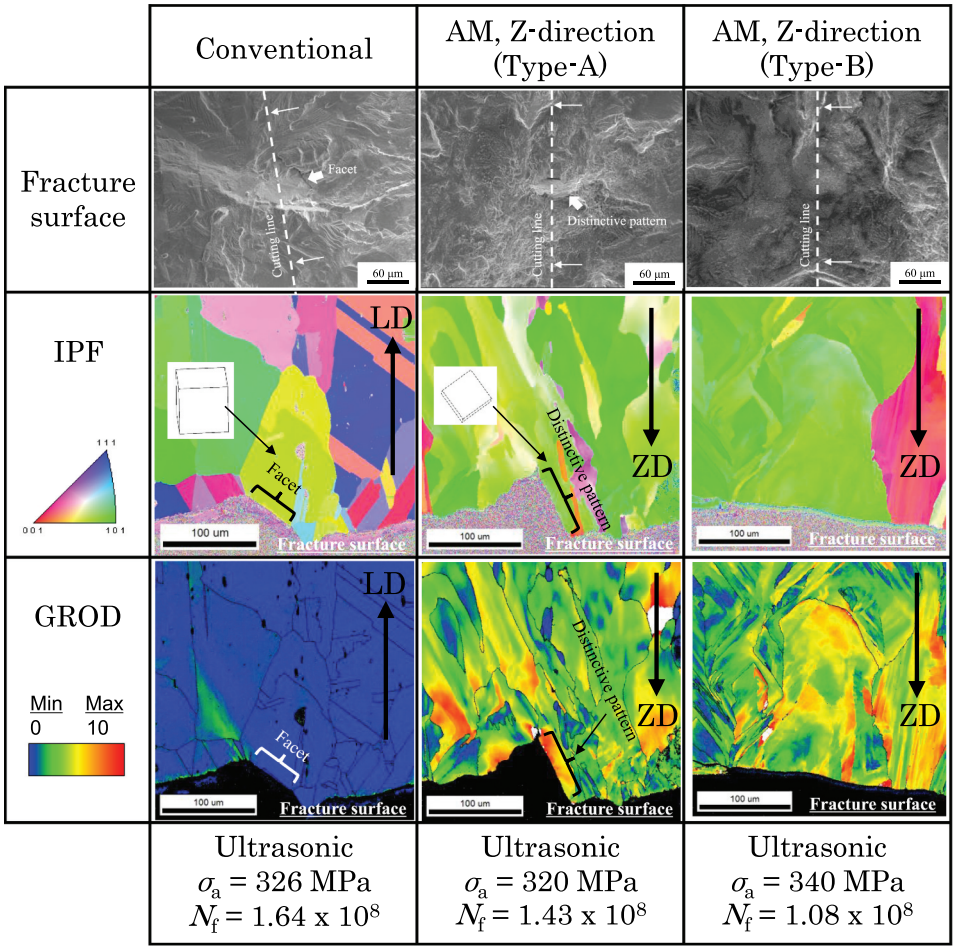

Figure 6. Results of cross-sectional EBSD analysis.

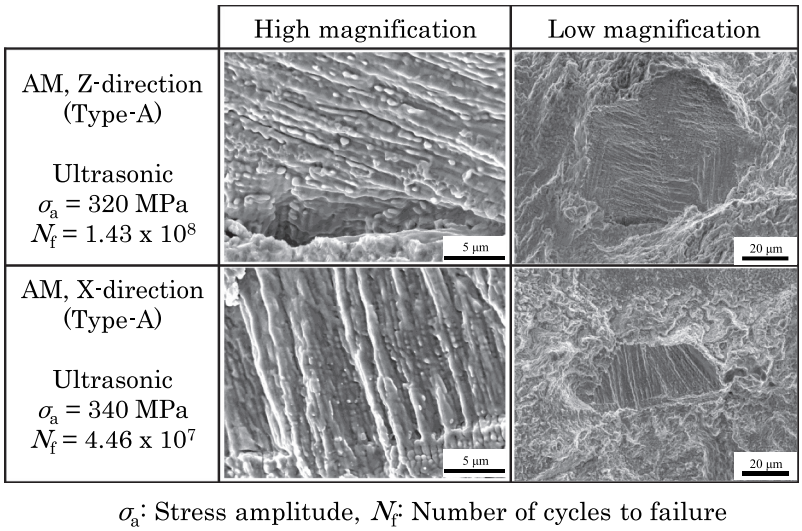

Figure 7. Detailed observations of distinctive patterns.

10^8 cycles. This result thus strongly suggests the presence of new fatigue limits in Hastelloy X.

The validity of the above discussion greatly depends on the reliability of the ultrasonic fatigue test results. The results for the AM samples in Figure 4 indicate that ultrasonic fatigue test results can be linked uninterruptedly to conventional HCF test results, supporting the validity of the ultrasonic fatigue test results. Although the results for conventional samples reveal a gap between the ultrasonic fatigue and HCF test results, this gap is caused by the low 0.2% proof stress of the conventional samples as discussed in Section 3.2. In short, this gap is unrelated to frequency effects. For these reasons, the ultrasonic fatigue test results can be considered reliable.

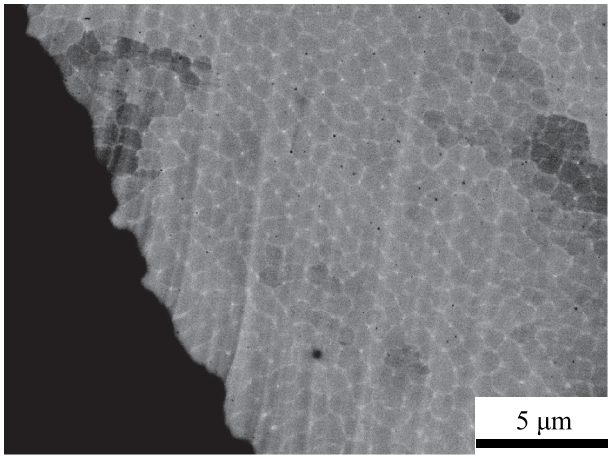

AM, Z-direction (Type-A)
(Ultrasonic, σ_a = 320 MPa, N_f = 1.43 x 10^8)

Figure 8. Microstructure beneath the distinctive pattern area.

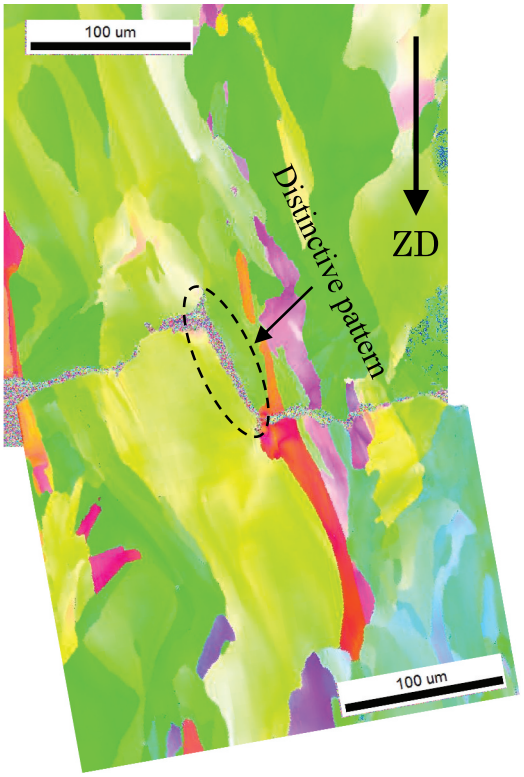

AM, Z-direction (Type-A)
(Ultrasonic, σ_a = 320 MPa, N_f = 1.43 x 10^8)

Figure 9. Matching the cross-sectional EBSD for the distinctive pattern. The specimen is the AM, Z-direction (Type A) shown in Figure 6.

4.2. Internal fracture mechanisms

The conventional samples revealed internal fracture mechanisms of the type typically seen in nickel-based superalloys. The internal fracture origins revealed facets that had been formed in the shear direction and on the {111} slip plane, suggesting that the internal fracture origins are shear-type fatigue cracks. Similar facets have been frequently observed at fatigue fracture origins in nickel-based superalloys [45,46].

The AM samples revealed two types of internal fracture origins: Type A and Type B. Type A revealed a distinctive pattern at the internal fracture origins, while Type B did not. The distinctive pattern area was formed in a more inclined direction than the facets in the conventional sample, meaning that the distinctive pattern area was not a shear-type fatigue crack. Moreover, the distinctive pattern area was formed at a grain boundary. These observations suggest the distinctive pattern area to be evidence of a history of solidification cracking [4]. In short, the distinctive pattern area derives from an initial defect formed in the AM samples. In Type B, the internal fatigue cracks are formed in a part of the matrix without defects, as established in the conventional sample. However, the mechanism of Type B is different from that seen in the conventional sample. Although the conventional sample revealed shear-type fatigue cracks at the internal fracture origins, Type B was a tensile type. The details of the mechanism remain unknown; however, it is possible that the texture and high internal plastic strain are responsible for different types of internal fatigue crack initiation.

It is established that the typical microstructural defects of AM metallic materials are porosity, lack of fusion, and solidification cracking [1]. In this study, only solidification cracking appeared at the fatigue fracture origins. In other words, porosity and lack of fusion did not cause fatigue failure. Hastelloy X is a low-strength, ductile material that is insensitive to defects. Small defects therefore do not affect the fatigue properties of Hastelloy X. Moreover, the simple single-phase microstructure of Hastelloy X is advantageous to minimizing the defect sizes. For this reason, porosity and lack of fusion had no deleterious effects on the AM Hastelloy X produced in this study.

5. Summary

In this study, we carried out gigacycle fatigue tests on AM Hastelloy X at room temperature. Two types of AM samples, manufactured in the Z- and X-direction, were fabricated to investigate the effects of direction of build. Conventional samples were also tested for comparison. We used both ultrasonic fatigue tests and conventional HCF tests. The conclusions obtained from these fatigue tests are listed below.

(1) Microstructures of the AM samples revealed a (101) texture and high internal plastic strain, in contrast to the random texture and negligible internal plastic strain seen in the conventional samples.
(2) 0.2% proof stresses of the AM samples were much higher than those of the conventional

samples. The AM X-direction sample showed higher strength and lower ductility than the AM Z-direction sample due to the (101) texture.

(3) Most of the ultrasonic fatigue tests ended in internal fractures at above 10^7 cycles, showing comparable results between the AM and the conventional samples. The difference between the Z- and X-direction samples was also minor.

(4) The HCF test results for the AM samples revealed longer fatigue lives than those of the conventional samples because of the high 0.2% proof stress of the AM samples. The difference between the directions of the AM sample was negligible.

(5) The ultrasonic fatigue test results of the AM samples were continuously connected to the HCF test results, supporting the validity of the ultrasonic fatigue test results.

(6) These results indicated conventional fatigue limits at 10^7 cycles to be absent in Hastelloy X, although the presence of new fatigue limits in gigacycle regions was suggested.

(7) Internal fracture origins of the AM samples consisted of two types. One showed a distinctive pattern, while the other did not. The internal fracture origins of the conventional samples were so-called 'facets'.

(8) The most distinctive pattern was a history of solidification cracking, a typical defect of AM metallic materials. In other words, other types of defects (porosity and lack of fusion), did not cause fatigue failure in the AM Hastelloy X.

Disclosure statement

No potential conflict of interest was reported by the author(s).

Funding

This study was supported in part by a grant from the Amada Foundation [No. AF-2022201-A3].

References

[1] Gorsse S, Hutchinson C, Gouné M, et al. Additive manufacturing of metals: a brief review of the characteristic microstructures and properties of steels, Ti-6Al-4V and high-entropy alloys. Sci Technol Adv Mater. 2017;18(1):584–610. doi: 10.1080/14686996.2017.1361305

[2] Leuders S, Thöne M, Riemer A, et al. On the mechanical behaviour of titanium alloy TiAl6V4 manufactured by selective laser melting: fatigue resistance and crack growth performance. Int J Fatigue. 2013;48:300–307. doi: 10.1016/j.ijfatigue.2012.11.011

[3] Li P, Warner DH, Fatemi A, et al. Critical assessment of the fatigue performance of additively manufactured Ti–6Al–4V and perspective for future research. Int J Fatigue. 2016;85:130–143. doi: 10.1016/j.ijfatigue.2015.12.003

[4] Aboulkhair NT, Simonelli M, Parry L, et al. 3D printing of aluminium alloys: additive manufacturing of aluminium alloys using selective laser melting. Prog Mater Sci. 2019;106:100578. doi: 10.1016/j.pmatsci.2019.100578

[5] Yadollahi A, Shamsaei N. Additive manufacturing of fatigue resistant materials: challenges and opportunities. Int J Fatigue. 2017;98:14–31. doi: 10.1016/j.ijfatigue.2017.01.001

[6] Uzan NE, Shneck R, Yeheskel O, et al. Fatigue of AlSi10Mg specimens fabricated by additive manufacturing selective laser melting (AM-SLM). Mater Sci Eng A. 2017;704:229–237. doi: 10.1016/j.msea.2017.08.027

[7] Blakey-Milner B, Gradl P, Snedden G, et al. Metal additive manufacturing in aerospace: a review. Mater Des. 2021;209:110008. doi: 10.1016/j.matdes.2021.110008

[8] Shrestha R, Simsiriwong J, Shamsaei N. Fatigue behavior of additive manufactured 316L stainless steel parts: effects of layer orientation and surface roughness. Addit Manuf. 2019;28:23–38. doi: 10.1016/j.addma.2019.04.011

[9] Cui L, Jiang F, Peng RL, et al. Dependence of microstructures on fatigue performance of polycrystals: a comparative study of conventional and additively manufactured 316L stainless steel. Int J Plasticity. 2022;149:103172. doi: 10.1016/j.ijplas.2021.103172

[10] Nishikawa H, Furuya Y, Kitano H, et al. In-situ observation of microstructurally small fatigue crack initiation and growth behaviors of additively-manufactured alloy 718. Mater Sci Eng A. 2022;835:142682. doi: 10.1016/j.msea.2022.142682

[11] Nishikawa H, Furuya Y, Kitano H, et al. Distinctive fatigue properties of additively-formed CoCrFeNiTiMo multi-principal element alloy: excellent fatigue crack growth resistance against ordinally high cycle fatigue strength. Mater Sci Eng A. 2024;891:145938. doi: 10.1016/j.msea.2023.145938

[12] Tusher MMH, Ince A. High cycle fatigue and very high cycle fatigue performance of selective laser melting Ti-6Al-4V titanium alloy—a review. Mater Perform Charact. 2023;12(2):214–293. doi: 10.1520/MPC20220088

[13] Siddique S, Imran M, Walther F. Very high cycle fatigue and fatigue crack propagation behavior of selective laser melted AlSi12 alloy. Int J Fatigue. 2017;94:246–254. doi: 10.1016/j.ijfatigue.2016.06.003

[14] Tridello A, Fiocchi J, Biffi CA, et al. VHCF response of Gaussian SLM AlSi10Mg specimens: effect of a stress relief heat treatment. Int J Fatigue. 2019;124:435–443. doi: 10.1016/j.ijfatigue.2019.02.020

[15] Yang K, Huang Q, Wang Q-Y, et al. Competing crack initiation behaviors of a laser additively manufactured nickel-based superalloy in high and very high cycle fatigue regimes. Int J Fatigue. 2020;136:105580. doi: 10.1016/j.ijfatigue.2020.105580

[16] Caivano R, Tridello A, Chiandussi G, et al. Very high cycle fatigue (VHCF) response of additively manufactured materials: a review. Fatigue Fract Eng Mater Struct. 2021;44(11):2919–2943. doi: 10.1111/ffe.13567

[17] Andrade MF, Pereira MV, Teixeira MC, et al. Fatigue life assessment in the very high cycle

regime of AISI 316L stainless steel processed by L-DED additive manufacturing. Procedia Struct Integrity. 2022;42:1008–1016. doi: 10.1016/j.prostr.2022.12.127
[18] Haghshenas M, Simsiriwong J. Very high cycle fatigue behavior of additively manufactured metals using ultrasonic fatigue testing: a critical assessment of potentials and challenges. Mater Perform Charact. 2023;12(2):186–196. doi: 10.1520/MPC20220090
[19] Furuya Y, Matsuoka S, Abe T, et al. Gigacycle fatigue properties for high-strength low-alloy steel at 100 Hz, 600 Hz, and 20 kHz. Scr Mater. 2002;46(2):157–162. doi: 10.1016/S1359-6462(01)01213-1
[20] Furuya Y, Hirukawa H, Takeuchi E. Gigacycle fatigue in high strength steels. Sci Technol Adv Mater. 2019;20(1):643–656. doi: 10.1080/14686996.2019.1610904
[21] Mason WP. Internal friction and fatigue in metals at large strain amplitudes. J Acoust Soc Am. 1956;28(6):1207–1218. doi: 10.1121/1.1908595
[22] Kuhn H, Medlin D. ASM handbook vol. 8, mechanical testing and evaluation. OH: ASM International; 2000.
[23] Ishii H, Yagasaki T, Akagi H. Evaluation of giga-cycle fatigue properties of some maraging steels by intermittent ultrasonic fatigue testing. Fatigue Fract Eng Mater Struct. 2002;25(8–9):831–835. doi: 10.1046/j.1460-2695.2002.00561.x
[24] Bathias C, Paris PC. Gigacycle fatigue in mechanical practice. New York: Marcel Decker; 2004.
[25] Mayer H. Recent developments in ultrasonic fatigue. Fatigue Fract Eng Mater Struct. 2016;39(1):3–29. doi: 10.1111/ffe.12365
[26] WES 1112. Standard test method for ultrasonic fatigue testing of metallic materials. 2017.
[27] Furuya Y, Shimamura Y, Takanashi M, et al. Standardization of an ultrasonic fatigue testing method in Japan. Fatigue Fract Eng Mater Struct. 2022;45(8):2415–2420. doi: 10.1111/ffe.13727
[28] Furuya Y, Abe T, Matsuoka S. 10^{10}-cycle fatigue properties of 1800 MPa-class JIS-SUP7 spring steel. Fatigue Fract Eng Mater Struct. 2003;46(7):641–645. doi: 10.1046/j.1460-2695.2003.00661.x
[29] Furuya Y, Nishikawa H, Hirukawa H, et al. Gigacycle fatigue properties of wrought aluminum alloys. Mater Perform Charact. 2023;12(2):63–77. doi: 10.1520/MPC20220082
[30] Furuya Y, Nishikawa H, Hirukawa H, et al. Takeuchi, fatigue properties of titanium alloys disclosed in NIMS fatigue data sheets. Sci Technol Adv Mater Methods. 2023;3(1):2285711. doi: 10.1080/27660400.2023.2285711
[31] Furuya Y, Kobayashi K, Hayakawa M, et al. High-temperature ultrasonic fatigue testing of single-crystal superalloys. Mater Lett. 2012;69:1–3. doi: 10.1016/j.matlet.2011.11.066
[32] Furuya Y. Small internal fatigue crack growth rate measured by beach marks. Mater Sci Eng A. 2016;678:260–266. doi: 10.1016/j.msea.2016.09.109
[33] Furuya Y. A new model for predicting the gigacycle fatigue strength of high-strength steels. Mater Sci Eng A. 2019;743:445–452. doi: 10.1016/j.msea.2018.11.109
[34] Furuya Y. Gigacycle fatigue of high-strength steel caused by MnS inclusions. Mater Sci Eng A. 2021;824:141840. doi: 10.1016/j.msea.2021.141840
[35] Kusano M, Watanabe M. Microstructure control of Hastelloy X by geometry-induced elevation of sample temperature during a laser powder bed fusion process. Mater Des. 2022;222:111016. doi: 10.1016/j.matdes.2022.111016
[36] Wang F. Mechanical property study on rapid additive layer manufacture Hastelloy® X alloy by selective laser melting technology. Int J Adv Manuf Technol. 2012;58(5–8):545–551. doi: 10.1007/s00170-011-3423-2
[37] Karapuzha AS, Fraser D, Schliephake D, et al. Room and elevated temperature tensile and fatigue behaviour of additively manufactured Hastelloy X. Mater Sci Eng A. 2023;882:145479. doi: 10.1016/j.msea.2023.145479
[38] Lei L, Li B, Wang H, et al. High-temperature high-cycle fatigue performance and machine learning-based fatigue life prediction of additively manufactured Hastelloy X. Int J Fatigue. 2024;178:108012. doi: 10.1016/j.ijfatigue.2023.108012
[39] Cheng J, Ryan D, Kemerling B, et al. Modeling low cycle fatigue (LCF) of additively manufactured Hastelloy X using an accelerated crystal plasticity fatigue damage model. Int J Fatigue. 2025;198:108980. doi: 10.1016/j.ijfatigue.2025.108980
[40] Karapuzha AS, Wegener T, Krochmal M, et al. Fatigue crack growth in additively manufactured Hastelloy X - influences of crack orientation and post-fabrication treatments. Mater Sci Eng A. 2022;854:143773. doi: 10.1016/j.msea.2022.143773
[41] Sawada K, Kimura K, Abe F, et al. Catalog of NIMS creep data sheets. Sci Technol Adv Mater. 2019;20(1):1131–1149. doi: 10.1080/14686996.2019.1697616
[42] Sawada K, Taniuchi Y, Sekido K, et al. Long-term creep properties of Ni-based 21Cr-18Fe-9Mo superalloys. Sci Technol Adv Mater Methods. 2023;3(1):2284129. doi: 10.1080/27660400.2023.2284129
[43] Kikuchi M. Elastic anisotropy and its temperature variation of single crystals of 18–12 type stainless steel. J Jpn Inst Met Mater. 1971;35(5):518–522. (in Japanese), doi: 10.2320/jinstmet1952.35.5_518
[44] Masumura T, Takaki S, Tsuchiyama T. Estimation of elastic stiffness in austenitic stainless steels. J Soc Mater Sci Jpn. 2021;70:31–34 (in Japanese), doi: 10.2472/jsms.70.31
[45] Nishikawa H, Habib K, Furuya Y, et al. Short fatigue crack growth mechanism in Ni-Co based superalloy at elevated temperatures and in oxidative atmospheres, Mater. Sci Eng A. 2023;885:145655. doi: 10.1016/j.msea.2023.145655
[46] Nishikawa H, Furuya Y, Osada T, et al. Three-dimensional high-resolution crystallographic observation of the entire volume of microstructurally small fatigue cracks in Ni-Co based superalloy. Scr Materialia. 2023;222:115026. doi: 10.1016/j.scriptamat.2022.115026
[47] Cui L, Jiang S, Xu J, et al. Revealing relationships between microstructure and hardening nature of additively manufactured 316L stainless steel. Mater Des. 2021;198:109385. doi: 10.1016/j.matdes.2020.109385
[48] Furuya Y. 10^{11} gigacycle fatigue properties of high-strength steel. ISIJ Int. 2021;61(1):396–400. doi: 10.2355/isijinternational.ISIJINT-2020-212